limitations on the result of this paper are that we use isotropic theory and an infinite medium. The mathematical complexities of the theory would be multiplied considerably if both these simplifications were not made. Finally, since the general formulas require closed dislocation loops, we close the helix with a return loop. This eliminates spurious and possibly misleading terms.

ACKNOWLEDGMENTS

The author wishes to express his sincere appreciation to Professor Frederick Seitz for suggesting this problem and for his guidance throughout the course of this work. He also wishes to thank Professor J. S. Koehler and Professor Robb Thomson for helpful discussions and suggestions.

PHYSICAL REVIEW VOLUME 116, NUMBER 3 NOVEMBER 1, 1959

Optical Absorption in Pure Single Crystal InSb at 298° and 78°K*

S. W. KURNICK† AND JOHN M. POWELL‡
Chicago Midway Laboratories, University of Chicago, Chicago, Illinois
(Received May 11, 1959)

The absorption spectra of single crystal homogeneous InSb were measured in the spectral range 5 to 10 microns at temperatures of 78°K and 298°K. Primary emphasis was placed on the precise determination of absorption coefficients less than 400 cm^{-1}. Absorption spectra were measured in many samples over the following range of impurity concentrations. Net impurity concentrations, expressed in atoms cm^{-3}, ranged from 5×10^{15} to 9.5×10^{16} in p-type samples, and from 2×10^{15} to 3×10^{17} in n-type samples, as determined from Hall coefficients measured at 78°K.

In general, the spectral range covered included regions where the absorption was dominated by either free-carrier absorption or valence-conduction band transitions. Free-carrier absorption in p-type InSb indicates a simple valence-band structure about $\mathbf{k}=0$, consisting of light and heavy hole bands. Free carrier cross sections at 298°K are $\sigma_p=8.65\times10^{-16}$ cm^2 per hole and $\sigma_n=0.23\times10^{-16}$ cm^2 per electron (at 9 μ). Whereas the free hole absorption coefficient is roughly independent of wavelength, the free electron absorption σ_n varies as λ^2 and agrees well with the classical Zener-Drude model.

The main absorption edge at both temperatures may be extended to lower absorption coefficients α by subtracting the extrapolated free carrier absorption coefficients α_c. The resultant band edge $\ln(\alpha-\alpha_c)$ values when plotted against the photoenergy ($\hbar\omega$) fits a straight line. The slopes of these band edges increase at the lower temperature and decrease (either at 78° or 298°K) as the acceptor concentration in the optical sample increases. Various models previously proposed are compared with the experimental results.

I. INTRODUCTION

THE measurement of infrared absorption is a standard procedure in studying certain properties of semiconductors. When applied to InSb, these measurements have yielded a reasonably clear picture of band structure and effective masses, free carrier absorption, and lattice vibrations.[1–6] In addition, many attempts were made to interpret the shape of the band edge,[7–9] and more recent studies have been made on the interaction of impurities (donors or acceptors) with the band structure itself.[10,11]

The purpose of our measurements was to evaluate the edge absorption and the free carrier absorption of InSb with more than ordinary emphasis upon the precise evaluation of absorption coefficients and the quality control of the semiconductor material. This detailed data on the absorption edge shape, as well as the shift in its effective cutoff, will be used to compare the various band edge interpretations.

II. EXPERIMENTAL DETAILS

A. InSb Samples

A summary of the InSb material used is shown in Table I. The samples were cut from large single crystals

TABLE I. InSb samples.

Specimen (see Figs. 3 and 4)	Net impurity concentration[a] (cm^{-3})	Mobility (cm^2/volt-sec)[b]	Total impurity concentration[c] (cm^{-3})
a	$2.07\times10^{17}n$	43 600	$2.1\times10^{17}n$
A	$2.95\times10^{17}n$	38 500	$3.0\times10^{17}n$
b, B	$2\times10^{15}n$	192 000	$4\times10^{15}n$
c	$2.75\times10^{16}p$	2900	$2.7\times10^{16}p$
C	$2.52\times10^{16}p$	3060	$2.5\times10^{16}p$
d, D	$9.5\times10^{16}p$	1650	$9.5\times10^{16}p$
E	$6.6\times10^{15}p$	4550	···

[a] Concentrations determined from Hall coefficient measurements at 78°K and defined as $1/eR_H$.
[b] Mobility determined from $R_H\sigma=\mu B$ at 78°K.
[c] Reference 12.

* This research was supported by the U. S. Air Force through the Office of Scientific Research of the Air Research and Development Command.

† Present address: John Jay Hopkins Laboratory for Pure and Applied Science, General Atomic Division of General Dynamics Corporation, San Diego, California.

‡ Now at Raulind Corporation, Chicago, Illinois.

[1] R. G. Breckenridge *et al.*, Phys. Rev. **96**, 571 (1954).
[2] M. Tanenbaum and H. B. Briggs, Phys. Rev. **91**, 1561 (1953).
[3] V. Roberts and J. Quarrington, J. Electronics **1**, 152 (1955).
[4] W. Kaiser and H. Y. Fan, Phys. Rev. **98**, 966 (1955).
[5] W. G. Spitzer and H. Y. Fan, Phys. Rev. **106**, 882 (1957).
[6] F. Oswald and R. Schade, Z. Naturforsch. **9a**, 611 (1954).
[7] Blount, Callaway, Cohen, Dumke, and Phillips, Phys. Rev. **101**, 563 (1956).
[8] R. F. Potter, Phys. Rev. **103**, 851 (1956).
[9] W. P. Dumke, Phys. Rev. **108**, 1419 (1957).
[10] F. Stern and R. M. Talley, Phys. Rev. **100**, 1638 (1955).
[11] F. Stern and J. R. Dixon, J. Appl. Phys. **30**, 268 (1959).

to minimize inhomogeneities; the crystals were grown by pulling from the melt. The samples ranged in impurity concentration from 5×10^{15} to 9.5×10^{16} acceptors cm^{-3}, and from 2.0×10^{15} to 3.0×10^{17} donors cm^{-3}. These values were determined from the Hall coefficient measured at 78°K by means of the relation $N_A-N_D=(eR_H)^{-1}$. At room temperature the carrier concentrations for the purer samples were essentially intrinsic with a concentration of 2×10^{16} carriers cm^{-3} in both the valence and conduction bands. The extent of compensation is of considerable interest. The tabulated mobilities are sufficiently high to indicate that compensation[12] is slight.

The crystals were sliced perpendicular to the direction of growth; each slice (about 1 sq inch in area) provided an optical blank $\frac{3}{4}$-inch in diameter and Hall measurement blanks from which was determined the extrinsic concentration of impurities at 78°K, and the uniformity of the transmission blank. (The N_A-N_D concentration was determined from the Hall coefficient measurements; the mobility[12] was used as an index to the amount of compensation.) Samples of measurable nonuniformity were rejected. Thickness of the optical blanks depended upon the requirements of the transmission measurements and ranged from 0.08 mm to 3 mm.

In the optical blank parallel surfaces were of great importance. To prepare the sample, low melting salol (40°C) was used to cement the sample to a steel block ground parallel to about 2 μ. The sample thus mounted was placed on the magnetic chuck of a surface grinder and ground to near-optical flatness with a 600-grit silicon carbide wheel. The surface was then optically polished by hand on a slightly convex pitch lap using 0.5 micron abrasive (Buehler Lts. 1551 AB) alumina in water with green soap. Then the salol was dissolved in methyl alcohol and the sample turned over, re-cemented, ground to the desired thickness and polished. Thickness was then measured and the sample checked for parallel surfaces, which were held to 0.0002 cm for thicker samples, and to 0.0001 cm for thinner ones. Flatness, checked with an optical flat, was within $\frac{1}{2}$ micron. To further insure against the effects of nonparallel surfaces, a stop was placed in the optical system to restrict illumination to the central area of the sample.

B. Optics

Transmission measurements were made with a double monochrometer (Beckman IR-3) which has been described by Donner.[13] The sample and cryostat were in the analyzed beam. The spectrophotometer optics were located in vacuum except for the thermocouple T_2 and its collecting mirror. These were placed in a dessicated plastic box (see Fig. 1). Following along the optical axis from the exit slit, the periscope plane mirrors M_1 and M_2 reflected the infrared beam to the spherical mirror M_3. The beam then passed through a doublet field lens M_4, then through the multiple cryostat windows (not shown in Fig. 1) and specimen S to the collecting mirror M_5 and finally to the thermocouple T_2. The field lens M_4 imaged the mirror M_3 on the sample. The spherical mirror M_3 focused the exit slit onto the field lens M_4. The collecting mirror M_5 focused the rays onto the collecting face of the thermocouple detector T_2. Great care was used to assure that the slit image remained on the thermocouple and that such small shifts as did occur did not interfere with measurement accuracy. (These shifts occurred when the cryostat window was removed for insertion of the blank and replaced.) The cryostat was vacuum-insulated, and the sample-chamber was arranged so that it could be filled with helium gas to effect heat exchange between the cooled walls and the sample. This arrangement requires four-vacuum-tight windows, two of which have to withstand cooling. The cryostat followed the design published by McMahon *et al.*,[14] but their spherical silver chloride windows and spherical seats were replaced by flat KRS-5 windows, teflon gaskets, and flat seats. The temperature of the sample was controlled to within 0.2°C.

C. Procedure of Transmission Measurements

A correction had to be applied to the recorded transmissions to compensate for the effect of multiple reflections between the many parallel surfaces of the cryostat windows. This effect was especially pronounced with KRS-5 windows, which had reflecting power per surface of 17%. Apparent transmissions were smaller than actual ones because the multiply-reflected rays that traverse the sample-space an odd number of times and contribute to the beam emerging toward the thermo-

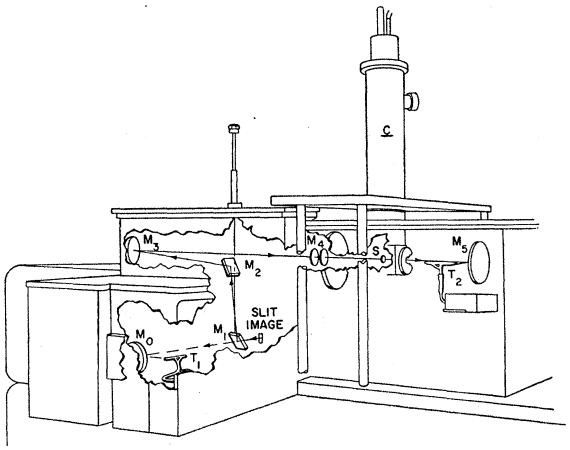

FIG. 1. Cut away view which shows the modified optical array of the Beckman IR-3 spectrophotometer and cryostat. Optical path starts from exit slit and terminates at detector T_2 at right.

[12] A. J. Strauss, J. Appl. Phys. **30**, 559 (1959).
[13] W. Donner, Electronics **28**, No. 11, 137 (1955).
[14] McMahon, Hainer, and King, J. Opt. Soc. Am. **39**, 786 (1949).

couple are attenuated on each passage through the sample. The difference between apparent and actual transmission was reduced by tilting the sample slightly (3°); analysis showed that with the tilted sample the apparent transmission T' and the true transmission T were related by the formula

$$1/T' = (1+a)/T - aT, \qquad (1)$$

where $a=0.089$ for KRS-5 windows. This correction was verified experimentally. When the T' was measured with KRS-5 windows and a sample, and then compared with the T measured without KRS-5 windows, the computed T from Eq. (1) agreed with the measured T to within $\frac{1}{2}\%$.

In the interpretation of the transmission data, care must be taken to allow for the influence of the slit width. The region in which the slit width plays a dominant role is that in which the transmission curve, as a function of wavelength (or photon energy) changes slope rapidly. Owing to the finite width of the slit and to diffraction, there will be overlapping of the slit images.[15] This source of error can be partially corrected, with accuracy of the correction depending on the slit width used. The best procedure, of course, is to use a slit so narrow that the error introduced is negligible. Unfortunately, for the longer wavelength region (5–10 μ) the problem of low signal levels sets a minimum to the narrowness of the slit available. A compromise was adopted by opening the slits somewhat and correcting for the overlap of slit images.

The measured transmission T' for the nominal slit width C_0 and wavelength λ determined the true transmission $T(\lambda)$ by the following relation:

$$T(\lambda) = T'(\lambda) - (1/12)\Delta^2 T'(\lambda) C_0^2 + \text{ascending difference terms}, \qquad (2)$$

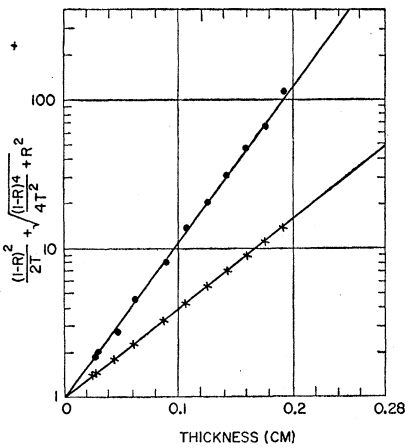

FIG. 2. Test for use of $R=0.35$ ($n=3.90$). The transmission T of a uniform sample was measured at two wavelengths beyond the cutoff as a function of thickness. The selection of $R=0.35$ is shown to be a proper fit by the linearity of the array of points.

[15] W. E. Forsythe, *Measurements of Radiation Energy* (McGraw-Hill Book Company, Inc., New York, 1937), p. 349.

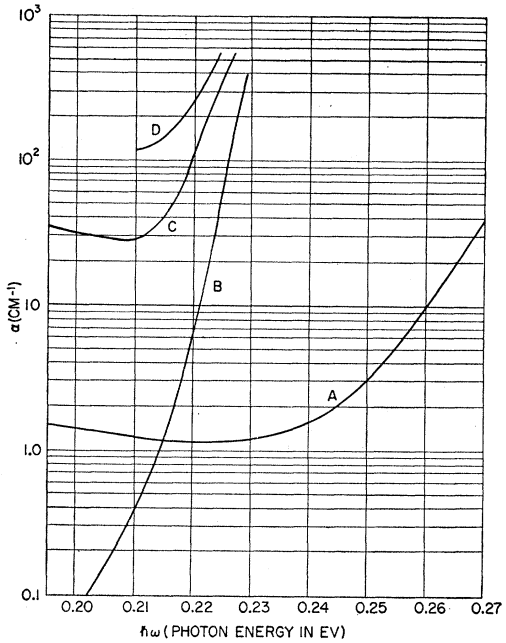

FIG. 3. The plot of $\ln\alpha$ *vs* $\hbar\omega$ (ev) at 78°K for samples of various extrinsic concentrations. Samples *A*, *B*, *C* and *D* are described in Table I.

where the difference term was

$$\Delta^2 T'(\lambda) = T'(\lambda+C_0) + T'(\lambda-C_0) - 2T'(\lambda).$$

To find the proper slit width C_0, runs were made with the resolving power as high as 0.0015 ev and compared with runs at a somewhat lower resolving power. The overlap correction [Eq. (2)] was applied to the lower resolution run, then compared with the transmittancies of the high resolution run. When the comparison showed no difference greater than 5%, the greater signal available with somewhat opened slits enabled measurements to be taken to higher absorption coefficients. The resolution used most frequently was about 0.0025 ev.

Since the reported values of the index of refraction of InSb range from 3.75 to 4.10, an independent value of R, the reflection coefficient, was determined from the transmission T as a function of thickness x. The best value for R was determined by plotting assumed values for R with the measured transmission *versus* the corresponding thickness. The criterion of linearity was used to determine R as 0.35 ($n=3.90$). Figure 2 shows $\ln\{[(1-R)^2/2T]+[R^2+(1-R)^4/4T^2]^{\frac{1}{2}}\}$ *vs* x for a p-type sample (Hall concentration 2.17×10^{15} carriers at 78°K) for two different wavelengths. Other samples of different concentrations were also measured in the same way and were found to be in agreement with the value selected.

The accuracy with which T could be measured as well as the range over which T could be measured for a given sample thickness determined the reliability of αx, the product of the absorption coefficient and thick-

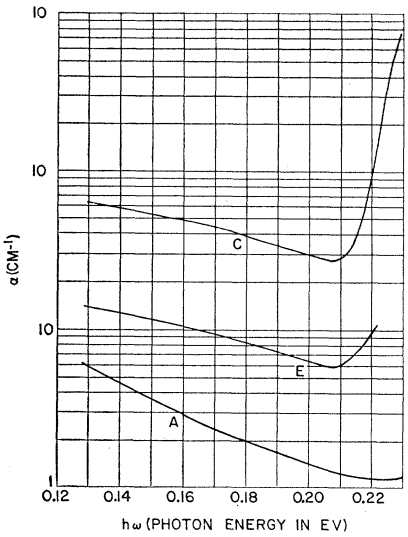

FIG. 4. Extension of Fig. 3 data to lower photon energies at 78°K. See Table I for sample data.

ness. Values of αx about 6.0 set the upper limit at which the Johnson noise of the thermocouple drowned out the transmitted signal. The lower limit $\alpha x = 0.02$ was determined by the accuracy of the value given to R. To obtain a reliably wide range of α's it was found important to use as many as several thicknesses for a sample.

III. RESULTS AND DISCUSSION

The absorption spectra for doped InSb samples at 298° and 78°K are shown in Figs. 3, 4, and 5. For extrinsic concentrations and mobilities see Table I. These curves are each characterized by the presence of a strong absorption edge towards the higher photon energies, and a relatively flat region towards the lower photon energies. At both temperatures the flat region is dominated by free carrier absorption and depends on the impurity concentration.

The steeply rising portion of the absorption curve will be interpreted in terms of transitions from the conduction band to the valence band. For the more highly doped n-type material the steeply rising band edge shows the Burstein effect.[16] This shift of the edge towards increased photon energies is ascribed to the filling of the bottom of the conduction band and is apparent at both 78° and 298°K (samples a, A).

A comparison of Roberts and Quarrington's data[3] with ours (Figs. 6 and 7) shows a sharper rise of our band edges at the same temperature. Furthermore, their data at temperatures below 78°K shows only a shift in the band edge and no change in shape. There is a possibility that their high curvature region could be interpreted as nothing more than the rounding off of absorption readings between the sharply falling portion and the flat portion (slit-width overlapping). Our data utilized slit-widths so small that the high curvature region may be interpreted as a definite property of the InSb absorption and not of the spectrophotometer slits.

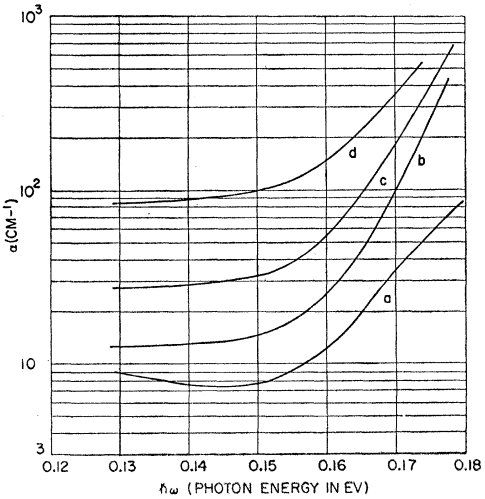

FIG. 5. The plot of $\ln\alpha$ *vs* $\hbar\omega$ (ev) at 298°K for samples of various extrinsic concentrations. Samples a, b, c, and d are described in Table I.

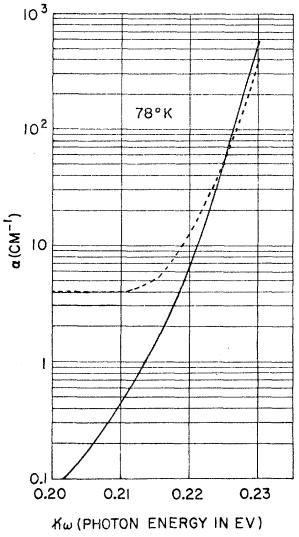

FIG. 6. Comparison of Roberts and Quarrington data (– –) with ours (——). Observations taken at 78°K.

A. Free Carrier Absorption

In Fig. 8 the free carrier absorption is shown as a function of the doping determined from 78°K Hall measurements. The photon wavelength at which the free carrier absorption was considered was 9 μ at 298°K and 8 μ at 78°K, just beyond the intrinsic absorption edge.

At 78°K the hole optical cross section is some 215 times greater than that of the conduction band electrons. However, the room temperature data requires more analysis. Assume that for the doping concentrations used, σ_p and σ_n, the hole and electron absorption

[16] E. Burstein, Phys. Rev. **93**, 632 (1954).

cross sections, are both independent of the impurity concentration; then the absorption constant is

$$\alpha=\sigma_p p_0+\sigma_n n_0. \tag{3a}$$

Furthermore, the mass action equation holds for slight impurity concentrations, and the equation for electrical neutrality gives.

$$n_0 p_0=n_i^2, \tag{3b}$$

$$p_0-n_0=N_A-N_D. \tag{3c}$$

Solve for p_0 and n_0 between Eqs. (3b) and (3c); then inserting the results in Eq. (3a) the absorption coefficient α_c is given directly in terms of N_A-N_D and n_i

$$\alpha_c=\tfrac{1}{2}(\sigma_p-\sigma_n)(N_A-N_D)+n_i(\sigma_p+\sigma_n)\left[1+\left(\frac{N_A-N_D}{2n_i}\right)^2\right]^{\frac{1}{2}}. \tag{4a}$$

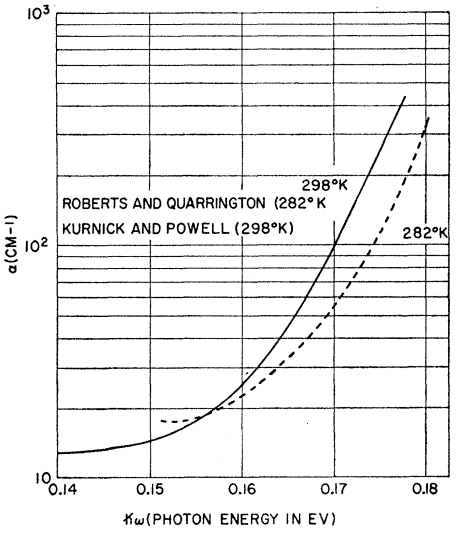

FIG. 7. Comparison of Roberts and Quarrington data (- - 282°K) with our data (—— 298°K).

When n_i, the intrinsic concentration, is sufficiently small, the hyperbolic plot of α *vs* (N_A-N_D) becomes so sharp at the origin, that Eq. (4a) breaks down into the two asymptotic solutions

$$\alpha=\sigma_p(N_A-N_D) \quad \text{and} \quad \alpha=\sigma_n(N_D-N_A). \tag{4b}$$

These conditions hold at 78°K when $n_i\sim 10^9$ cm^{-3}.

At 298°K the ratio $(N_A-N_D)/2n_i$ is no longer large compared to unity and the absorption curve is hyperbolic. To test the two asymptotes, contours were drawn for $n_i=2\times10^{16}$ cm^{-3} and 1×10^{16} cm^{-3} where the α's were calculated using the values of σ_p and σ_n of the asymptotic slopes (see Fig. 9).

The best fit is that for $n_i=1.5\times10^{16}$, which is close to the accepted value $n_i=2\times10^{16}$ cm^{-3} at 298°K. From the asymptotic slopes $\sigma_p=8.65\times10^{-16}$ cm^2 and $\sigma_n=0.23\times10^{-16}$ cm^2 and their ratio is about 40. That the

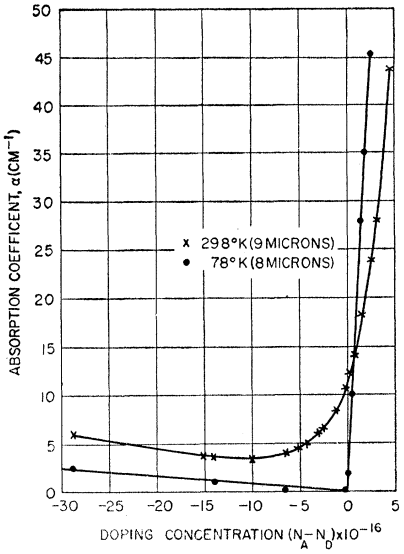

FIG. 8. Absorption coefficient *versus* extrinsic doping as determined by 78°K Hall coefficient measurements. The temperatures at which these measurements were made were 298°K and 78°K.

asymptotes have different slopes at different temperatures shows that the scattering mechanism does not remain the same. Whereas the free hole cross sections did not vary with photon energy, those for the more heavily doped *n*-type material did increase according to a λ^2 dependency.[1]

As a check on the observed absorption cross sections of the conduction band electrons, the effective mass

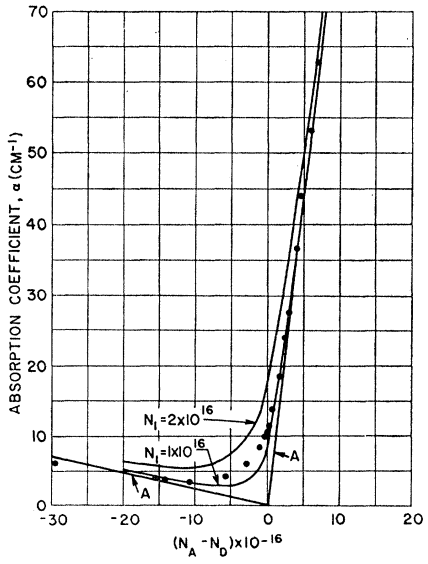

FIG. 9. Analysis of 298°K absorption coefficients *versus* extrinsic concentration as determined from Hall coefficient data taken at 78°K. The asymptodes A and A' were first drawn in to determine σ_n and σ_p, the optical cross sections. The two curves drawn for $n_i=1\times10^{16}$ and 2×10^{16} cm^{-3} bracket the observed concentration. Best fit is determined by $n_i=1.5\times10^{16}$ cm^{-3} at 298°K. The symbol A on the right-hand side of the figure should read A'.

may be calculated from the Zener-Drude model[17] in which

$$\sigma_n=\frac{e^3\lambda^2}{nc^3m^{*2}\mu}, \tag{5}$$

the mobility $\mu=e\tau/m^*$ is introduced after converting 7.6×10^4 cm^2 volt^{-1} sec^{-1} to esu. The effective mass ratio $m^*/m=0.025$ is derived for $\lambda=9$ microns in good agreement with the effective mass derived by other methods.

For p-type material, the shape of the free hole absorption *vs* photon energy $\hbar\omega$ is flat.[1] This obviously different functional dependence of the absorption on $\hbar\omega$ can be tested for a valence band structure similar to that proposed for p-type Ge by Kahn.[17] His model for p-type Ge utilized a simple band structure about $\mathbf{k}=0$ of both heavy and light hole bands. The free hole absorption was attributed to scattering between these valence bands.

If one uses the same model for p-type InSb and calculates the absorption coefficient at 298°K for the free holes, then $\sigma_p=3\times10^{-16}$ cm^2 at 9 μ, with the assumed heavy hole mass $0.20m$ and the assumed light hole mass $0.03m$. This is to be compared with the measured value $\sigma_p=8.6\times10^{-16}$ cm^2.

B. Edge Absorption

The shift of the band edge towards higher photon energies as the sample becomes more and more n-type has been previously interpreted (Burstein effect[16]). However, there is another shift of the band edge in the p-type material which moves the edge farther into the infrared with higher acceptor doping. If the extrapolated free carrier contribution α_c is subtracted from the observed α's close to the more strongly absorbing band edge, the plot of the absorption edge $\ln(\alpha-\alpha_c)$ *vs* $\hbar\omega$ may be approximated by a straight line. This is demonstrated in Fig. 11 for samples b', B' and c', C' at both temperatures (see Table I). The quantity $\ln(\alpha-\alpha_c)$ shows two definite trends: (1) as the sample becomes more and more p-type, the band edge slope becomes less steep; (2) the band edge for a given concentration becomes steeper upon cooling to 78°K. Except for the dependency of the slope of the band edge upon the acceptor concentration, the temperature behavior of the absorption data varies approximately as

$$\alpha=\alpha_0\exp[\hbar(\omega-\omega_0)/kT]. \tag{6}$$

Urbach[18] has noted similar behavior in the silver halides and a number of other crystals. However, there has been no detailed analysis available as to why the absorption should follow Eq. (6). This effect was first observed by Roberts and Quarrington[3] and an attempted interpretation was made by Stern and Talley[10] on the limited evidence available. They explained the shift to be due to hydrogenic impurities interacting with the band edge. For this shift to occur the impurity concentration must be so large that impurity levels are no longer well separated from the main band edge. Their criterion for the minimum concentration was

$$N_{\min}=3\times10^{23}(m_{\text{eff}}/m_K)^3 \text{ cm}^{-3}.$$

For p-type and n-type InSb their computed threshold concentrations were $N>5.0\times10^{17}$ acceptors cm^{-3} and $N>2\times10^{15}$ cm^{-3}. With such a low concentration requirement the shift should be noticeable for n-type material, if it were not for the larger shift of the cutoff towards the visible (Burstein effect). The p-type InSb samples used in our experiments do not fulfill the compensation requirements. The p-type samples are not compensated sufficiently (see Table I). However, a bigger objection is that the shift of the band edge towards lower photon energies increases well below 5×10^{17} acceptors cm^{-3}.

Another objection may be raised as to whether the lowest energy level of the band is sufficient to interpret a model. The distribution of the density of states in the bands should also be considered.

There are many imperfection types which may cause the edge of the cutoff to spread into the forbidden band: dislocations, impurity atoms, and lattice vibrations (acoustical and optical modes).[19] The common characteristic of these imperfections is their ability to break down the selection rules of the host crystal. Ordinarily, the host crystal, without imperfections, would comply with direct transitions in which an exciting photon would kick an electron across the gap with conserva-

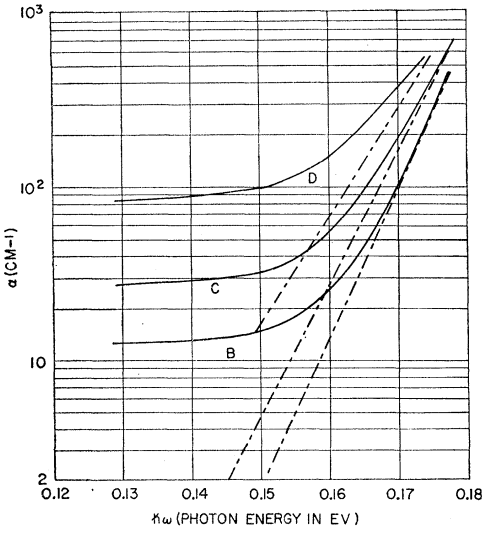

FIG. 10. Subtraction of the extrapolated free-carrier absorption from the absorption coefficients near the band edge results in an extended linear plot of $\ln(\alpha-\alpha_c)$ *vs* $\hbar\omega$. Shown resolved are 298°K data of samples *b*, *c*, and *d*.

[17] A. H. Kahn, Phys. Rev. **97**, 1647 (1955).
[18] F. Urbach, Phys. Rev. **92**, 1324 (1953).
[19] D. L. Dexter, *Proceedings of the Conference on Photoconductivity, Atlantic City, 1954*, edited by R. G. Breckenridge, *et al.* (John Wiley & Sons, New York, 1956).

tion of wave number between the initial and final states as well as conservation of energy. The shape of the band edge for such direct transitions, according to Bardeen, Blatt, and Hall would be precipitously steep.[20] The cause for spreading of the absorption edge has then been ascribed to indirect transitions aided by phonons.

By an indirect transition we mean a second order transition through a virtual intermediate state which involves scattering in $\mathbf{k}$ space by the absorption or emission of a phonon in addition to the usual absorption of a photon. The breakdown in the selection rule, in this case, occurs when $\mathbf{k}'-\mathbf{k}=\mathbf{q}$, the phonon momentum. Such a model where both the valence and the conduction band extrema occur at $\mathbf{k}=0$, has been proposed by Dumke.[9] This section will emphasize the detailed analysis of the band edge shapes where the indirect transitions play an important role.

As an example, Fig. 11 shows semilog plots of the measured absorption coefficients *vs* photon energy which are to be compared in shape with that computed from other models. A semilog plot was selected to compare shapes since the models proposed only provide the relative absorption coefficients and not their absolute values. The contribution from the free carriers has already been subtracted away. Figure 11 shows more plots of the 78°K data with the residual absorption subtracted away. Band edge shape of Dumke's optical mode model is to be compared with our experimental data. An additional interpretation utilizing a screened potential is also shown for comparison. See Appendix I for the analysis of the screened potential model. It is to be pointed out that the absorption curve is steepened at 78°K. At 298°K the shape is adequate and the proposed models appear consistent for the optical mode with an equivalent temperature. However, unexplained is the temperature and acceptor density dependency.

ACKNOWLEDGMENTS

The authors wish to acknowledge the aid and encouragement of F. F. Rieke who made many valuable suggestions during the course of the work.

APPENDIX I

Of further interest is the application of phonon-electron interaction for interpretation of the tail of the absorption band edge. Dumke[9] has utilized a simple band structure with extrema at $\mathbf{k}=0$ to interpret the band edge shape by an indirect transition mechanism.

$$\alpha=\frac{2}{(2\pi)^4}\frac{e^2\hbar\langle|P_{vc}|^2\rangle_{\mathrm{Av}}}{ncm^2\Delta Eg}\int d^3k\int d^3k'\times\frac{|H_{kk'}|^2\delta[\Delta E+(\alpha_v k^2+\alpha_c k'^2)\hbar^2/2m-\hbar\omega-k\theta]}{[\Delta E+(\alpha_v+\alpha_c)\hbar^2k^2/2m-\hbar\omega]^2}.$$

The square of the momentum operator $\langle|P_{vc}|^2\rangle_{\mathrm{Av}}$ was averaged between the valence and conduction band over all directions of polarization of the phonons. The other matrix $H_{kk'}$ was the element for scattering between k and k' in the valence band by absorption of a phonon of energy $k\theta$.

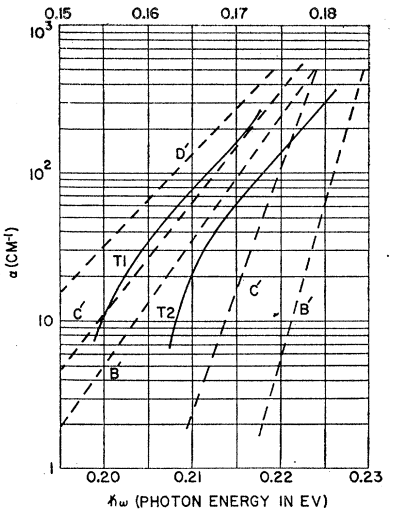

FIG. 11. Comparison of resolved band edge shapes at both 78°K (B' and C') and 298°K (b', c', and d'). Edge shapes of proposed models are T_1 and T_2. In Dumke's analysis, T_1 the scattering potential $|H_{kk'}|^2$ is taken to be constant and independent of $\mathbf{k}$ and $\mathbf{k}'$. An extension of Dumke's analysis to a screened scattering potential is shown by curve T_2. *Note.*—The symbol D' in the figure should read d'. The symbol B' in the lower left-hand corner of the figure should read b'.

The scattering matrix on which Dumke based his conclusions was $|H_{kk'}|^2=|\beta^2|(\exp\theta/T-1)^{-1}$ where $|\beta^2|$ is independent of $\mathbf{k}'$ and $\mathbf{k}$. The absorption coefficient

$$\alpha=\frac{A}{e^{\theta/T}-1}\left[\frac{\varphi}{(\varphi^2-1)^{\frac{1}{2}}}-1\right],$$

where

$$A=\frac{4}{\pi}\frac{e^2m|\beta^2|\langle|P_{vc}|^2\rangle_{\mathrm{Av}}}{nch^5\Delta E(\alpha_v\alpha_c)^{\frac{3}{2}}(1+\alpha_c/\alpha_v)^2},$$

and

$$\varphi-1=\frac{2}{1+\alpha_c/\alpha_v}\left\{\frac{k\theta}{\hbar\omega+k\theta-\Delta E}-1\right\}.$$

His conclusions for the best fit of the Roberts and Quarrington data at different temperatures was the selection of the ratio of the effective masses $\alpha_c/\alpha_v=5$. Inserting $k\theta=290$°K, the relative absorption coefficient was computed and is to be compared with the experimental band edge curves for shape in Fig. 11.

Another form for the scattering matrix included the effects of polarization by the optical phonons and the screening by other mobile carriers.[21] Inserted for $|H_{kk'}|^2$ was

$$|H_{kk'}|^2=\frac{|\Gamma^2|}{e^{\theta/T}-1}\frac{(\mathbf{k}-\mathbf{k}')^2}{[(\mathbf{k}-\mathbf{k}')^2+b^2]^2},$$

where $b^2=4\pi e^2(n_0+p_0)/n^2kT$ is the reciprocal square of

[20] Hall, Bardeen, and Blatt, Phys. Rev. **95**, 559 (1954).

[21] H. Ehrenreich, J. Phys. Chem. Solids **2**, 131 (1957).

the Debye-Hückel screening length and $|\Gamma^2|$ is independent of $\mathbf{k}$ and $\mathbf{k}'$. The results will differ from Dumke's nomenclature only in the interchange of α_v and α_c to consider hole instead of electron transitions because of the many more states in the valence band.

After some mathematical manipulations

$$\alpha=\frac{1}{(2\pi)^2}\frac{e^2\langle|P_{vc}|^2\rangle_{Av}}{nc\hbar^3\Delta Ek\theta}\frac{|\Gamma^2|(e^{\theta/t}-1)^{-1}\mathcal{J}}{(1+\alpha_v/\alpha_c)^2\alpha_v\alpha_c},$$

where the term $\mathcal{J}$ was found to equal

$$\mathcal{J}=4\pi\left(\frac{1-\psi}{1+\psi}\right)^{\frac{1}{2}}(\varphi+\psi)\frac{\partial}{\partial\Phi}\left[\frac{\Phi-1}{\Delta}\left\{\frac{\varphi\Phi+\psi}{(\varphi^2-1)^{\frac{1}{2}}}-(\Phi^2-1)^{\frac{1}{2}}\right\}\right],$$

the terms ψ, φ, Φ, and Δ were defined as

$$\psi=\frac{1-\alpha_v/\alpha_c}{1+\alpha_v/\alpha_c},$$

$$\varphi+\psi=(1+\psi)\frac{k\theta}{\hbar\omega+k\theta-\Delta E},$$

and

$$\Delta=(\Phi+\varphi\psi)^2+(\varphi^2-1)(1-\psi^2).$$

In Fig. 11, the computed shape of α (in relative units) *vs* the photon energy $\hbar\omega$ is shown for the two cases $b^{-1}=2\times10^6$ cm^{-1} for $(n_0+p_0)=4\times10^{16}$ cm^{-3} and $\alpha_v/\alpha_c=0.1$ and for the case $|H_{kk'}|^2=|\beta^2|/(e^{\theta/T}-1)$.

PHYSICAL REVIEW VOLUME 116, NUMBER 3 NOVEMBER 1, 1959

Nordheim's Theory of the Resistivity of Alloys

GEORGE L. HALL
RIAS, Baltimore, Maryland
(Received June 8, 1959)

Nordheim's theory is extended to account for (1) ionic potentials that extend outside the unit cell, and (2) order of any range. It is shown that the original theory is less approximate than is generally asserted. As an incidental result, it is also shown that Flinn's electronic theory of order can be extended appreciably.

INTRODUCTION

IT is generally recognized that Nordheim's theory[1] of the resistivity of binary alloys that form continuous solid solutions has only a qualitative significance. Nevertheless there still seems to be an interest[2,3] in this theory, probably because no acceptable theory has been published except for dilute solutions. It therefore should be of interest to prove, as is done in this note, that the usual form of the theory, say Jones',[3] is less approximate than is usually asserted [Jones' equation (25.6) is exact]. The theory is also easily extended: (1) to account for ionic potentials that extend outside the unit cell, and (2) to account for order of any range.

In order to prove these facts, the order parameter of Cowley[4] is introduced using essentially Flinn's notation from his article[5] on the electronic theory of local order. (It is also incidentally proved that three of Flinn's approximations exactly cancel.)

THEORY: AN EXTENSION OF NORDHEIM'S THEORY OF THE RESISTIVITY OF BINARY ALLOYS

We imagine a disordered lattice of A- and B-atoms. Let the rigid potential associated with an A-atom be $U_A(\mathbf{r})$ and that associated with a B-atom be $U_B(\mathbf{r})$, where both $U_A(\mathbf{r})$ and $U_B(\mathbf{r})$ do not necessarily vanish outside the unit cell. Then the total potential $U(\mathbf{r})$ is given by

$$U(\mathbf{r})=\sum_{A\text{-atoms}}U_A(\mathbf{r}-\boldsymbol{\tau})+\sum_{B\text{-atoms}}U_B(\mathbf{r}-\boldsymbol{\tau}). \quad (1)$$

In order to decompose this into a more workable form, we introduce a function C_τ defined at the lattice points as follows:

$$C_\tau=m_B, \text{ if an } A\text{-atom is at } \boldsymbol{\tau}$$
$$=-m_A, \text{ if a } B\text{-atom is at } \boldsymbol{\tau},$$

where m_i is the concentration of the ith component. Further, we define an average potential

$$U_1(\mathbf{r})=\sum_\tau\{m_AU_A(\mathbf{r}-\boldsymbol{\tau})+m_BU_B(\mathbf{r}-\boldsymbol{\tau})\}, \quad (2)$$

which is periodic, and a "difference potential"

$$U_2(\mathbf{r})=\sum_\tau C_\tau\{U_A(\mathbf{r}-\boldsymbol{\tau})-U_B(\mathbf{r}-\boldsymbol{\tau})\}$$
$$=\sum_\tau C_\tau\Delta U(\mathbf{r}-\boldsymbol{\tau}), \quad (3)$$

which is disordered. Clearly, we have that

$$U(\mathbf{r})=U_1(\mathbf{r})+U_2(\mathbf{r}). \quad (4)$$

We next imagine we have the exact Bloch functions for the average potential (2) and then perturb these

[1] L. Nordheim, Ann. Physik **9**, 607 (1931).
[2] N. V. Grum-Grzhimailo, Fiz. Metal. i Metalloved. Akad. Nauk S.S.S.R. Ural. Filial **5**, 23–29 (1957).
[3] H. Jones, *Handbuch der Physik* edited by S. Flügge (Springer-Verlag, Berlin, 1956), Vol. 19, p. 269.
[4] J. M. Cowley, Phys. Rev. **77**, 669 (1950).
[5] P. A. Flinn, Phys. Rev. **104**, 350 (1956).